# Investigation of direct capture in the $^{23}$Na$(p, \gamma)^{24}$Mg reaction

A. Boeltzig,[1] R. J. deBoer,[2,*] Y. Chen,[2] A. Best,[1] M. Couder,[2] A. Di Leva,[1] B. Frentz,[2] J. Görres,[2] Gy. Gyürky,[3]
G. Imbriani,[1] M. Junker,[4] Q. Liu,[2] S. Lyons,[2,†] K. Manukyan,[2] K. T. Macon,[2,‡] L. Morales,[2] M. T. Moran,[2] D. Odell,[5]
C. Seymour,[2] G. Seymour,[2] E. Stech,[2] B. Vande Kolk,[2] and M. Wiescher[2]

[1]*Dipartimento di Fisica "E. Pancini", Università degli Studi di Napoli "Federico II" and Istituto Nazionale di Fisica Nucleare,
Sezione di Napoli, Complesso Universitario di Monte Sant'Angelo, Via Cintia 21, 80126 Napoli, Italy*
[2]*The Joint Institute for Nuclear Astrophysics, Department of Physics, University of Notre Dame, Notre Dame, Indiana 46556, USA*
[3]*Institute for Nuclear Research (Atomki), P.O.B. 51, H-4001 Debrecen, Hungary*
[4]*National Laboratory of Gran Sasso, Istituto Nazionale di Fisica Nucleare, 67010 Assergi, Italy*
[5]*Institute of Nuclear and Particle Physics and Department of Physics and Astronomy, Ohio University, Athens, Ohio 45701, USA*

The $^{23}$Na$(p, \gamma)^{24}$Mg reaction plays an important role in the nucleosynthesis of elements in the hot bottom burning environment of asymptotic giant branch stars by providing a breakout path from the NeNa cycle to the MgAl cycle. At temperatures above $\approx 0.06$ GK, the underlying nuclear reaction contributions to the rate are primarily narrow resonances, but at lower temperatures direct and broad resonance tail contributions come to dominate. While there have been recent studies to improve the uncertainties associated with these narrow resonances, little attention has been paid to the nonresonant component. In this work, experimental measurements are reported over the energy range from 0.5 and 1.05 MeV proton beam energy, with a focus on studying the off-resonance region of the cross section. Several transitions were observed where two broad resonances dominate the energy range and whose low energy tails contribute strongly to the low-energy, nonresonant, cross section. In addition, a clear signature of direct capture has been observed for the first time in the $^{23}$Na$(p, \gamma)^{24}$Mg reaction.

## I. INTRODUCTION

The $^{23}$Na$(p, \gamma)^{24}$Mg reaction is an important breakout link from the NeNa cycle [1] to the MgAl cycle [2]. These cycles require higher temperature environments and may operate in hydrogen shell burning of massive stars [3] or in hot bottom burning of asymptotic giant branch (AGB) stars [4] or in explosive hydrogen environments such as ONe novae, where the reaction link may affect the production of long-lived $^{22}$Na and $^{26}$Al nuclei [5]. A recent study of the reaction at the Laboratory for Underground Nuclear Astrophysics (LUNA) at the Istituto Nazionale di Fisica Nucleare (INFN) Laboratori Nazionali del Gran Sasso (LNGS) probed the low energy resonant reaction contributions in the proton energy range between 130 and 400 keV [6]. The strengths of three resonances at 140, 251, and 309 keV were determined. These contributions are expected to dominate the reaction rate for the temperature range associated with hot bottom hydrogen burning and explosive hydrogen burning.

This work focuses on additional reaction contributions associated with direct radiative capture (DC) to bound states in $^{24}$Mg and the low energy tails of broad resonances at $E_{\text{c.m.}} =$

840 keV ($E_x = 12.53$ MeV, $1^+$) and 980 keV ($E_x = 12.67$ MeV, $2^-$), as well as possible interference patterns tailing into the low energy range of interest. The $^{23}$Na$(p, \gamma)^{24}$Mg reaction in this energy range has been studied from 250 to 2500 keV by Switkowski *et al.* [7] and above 500 keV by Baxter *et al.* [8] and Leccia *et al.* [9]. Higher energy resonances between 1 and 2 MeV have been studied by Mourad *et al.* [10], Meyer *et al.* [11], and Endt *et al.* [12]. These earlier measurements focused on the determination of resonance strengths, while in this study the aim is to characterize the off-resonance energy dependence, DC, and interference effects, using *R*-matrix and DC model techniques to estimate their contributions to the stellar reaction rate.

The search for strong direct contributions to the $^{23}$Na$(p, \gamma)^{24}$Mg reaction is greatly aided by previous studies of the single-particle strength of bound states in the $^{24}$Mg compound system. In particular Refs. [13–16] used $(d, n)$ and $(^3\text{He}, d)$ transfer reaction cross sections in combination with the distorted wave Born approximation (DWBA) to determine proton spectroscopic factors ($C^2S$). When combined with the DC potential model formalism of Rolfs [17], the strongest DC transitions can be identified as shown in Fig. 1. While these calculations provide a good starting point for a study, they have large uncertainties associated with them ($\approx 50\%$), necessitating the direct measurement of the $^{23}$Na$(p, \gamma)^{24}$Mg cross sections if an improved level of uncertainty is to be achieved.

In this work, low energy $S$ factors are estimated using two different phenomenological models, each associated with the analysis of different types of reaction data. For the analysis

---

*rdeboer1@nd.edu

†Present address: Pacific Northwest National Laboratory, Richland, WA.

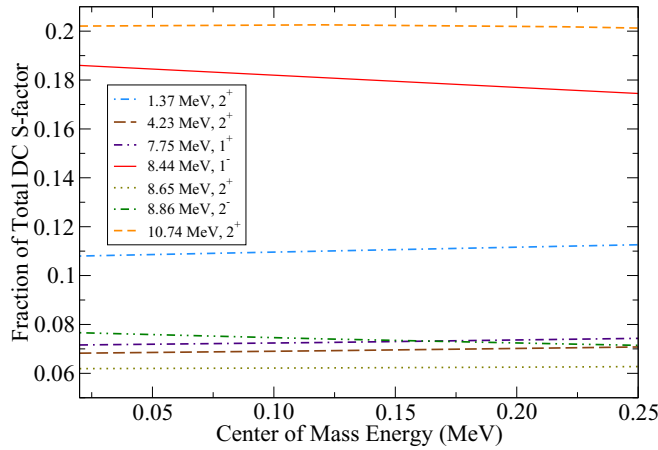‡Present address: InstroTek, 1 Triangle Dr., Research Triangle Park, NC 27709.

FIG. 1. Fractional contribution of the individual DC transitions to the total DC $S$ factor. Only those transitions that contribute more than 5% to the total are shown. The calculations used the $C^2S$ values from Garrett *et al.* [16].

of the capture cross sections measured in this work, the phenomenological $R$ matrix [18] along with the external capture model (EC) [19–22] is used to fit the experimental data and then extrapolate the $S$ factor to low energies. The strength of the EC is often characterized by the asymptotic normalization coefficient (ANC). Here the "off-resonance" $S$ factor is determined by the combination of the EC and tails of resonance contributions. These tail contributions are divided into those from actual resonances in the region of the data and those from background levels that mimic the summed contributions from all higher energy states. The largest uncertainties are often from incomplete knowledge of the level structure between the experimental data and threshold as well as contributions form the tails of higher lying resonances.

For transfer reactions, DWBA has been traditionally used to extract spectroscopic factors from forward angle angular distributions. A potential model can then be used, making sure to use the same potential parameters as the original DWBA analysis, to derive a single-particle direct capture (DC) cross section, which is weighted by the isospin Clebsch-Gordan factor [17]. Here the largest uncertainties in the calculated $S$ factors often come from uncertainties in the phenomenological potential model parameters. It is also now common practice to instead derive an ANC directly from the DWBA analysis [23]. However, the present analysis relies on $C^2S$ values from older work where this was not the case. Thus the $R$-matrix calculations and potential model calculations are performed separately and the comparison is made at the level of the off-resonance $S$ factors.

In the following, we will first discuss the experimental setup in Sec. II and results in Sec. III before we come to the detailed $R$-matrix (Sec. IV) and Markov chain Monte Carlo (MCMC) uncertainty (Sec. IV A) analysis of the low energy reaction cross section. The DC calculations are then described in Sec. V. A discussion of the results and revised reaction rates are given in Sec. VI with summary statements in Sec. VII.

## II. EXPERIMENTAL SETUP

The experiment was performed at the University of Notre Dame Nuclear Science Laboratory (NSL) using the Stable ion Accelerator for Nuclear Astrophysics (Sta. ANA), a 5 MV single-ended Pelletron accelerator, to produce proton beams between 0.5 and 1 MeV with maximum beam intensity on target of 15 $\mu$A. Targets were produced by evaporating $Na_2WO_4$ onto a 0.5 mm thick Ta backing, which also served as a beam stop, and which was electrically isolated from the rest of the beam line. The target, mounted at 45° degrees relative to the beam direction, was water cooled in order to reduce degradation due to heating. A circular copper tube was mounted inside the beam line, which extended from a cold head to within a few millimeters of the target face. The copper tube was both cooled with liquid nitrogen and biased to $-300$ V, acting simultaneously as a cold trap and electron suppressor.

The detector system consisted of a single, high efficiency (120% relative efficiency), high purity, co-axial germanium detector (HPGe). The detector was mounted on a rail system at an angle of 45° relative to the beam. The rail system allowed the detector to be easily moved to different distances from the target in order to make summing correction measurements during the calibration. Measurements of the $^{23}Na(p, \gamma)^{24}Mg$ cross section were taken in close geometry.

## III. DATA ANALYSIS

The full-energy peak detection efficiency of the HPGe detector was determined with calibration sources of known activity ($^{60}Co$ and $^{137}Cs$), and the $E_p = 992$ keV resonance in the $^{27}Al(p, \gamma)^{28}Si$ reaction, which has a well-known strength and branching ratios [24]. The efficiency, as a function of energy and distance, was parametrized empirically [25] and fitted to the measurements at different detector distances, accounting for summing in and summing out. The observed full-energy peak efficiencies (with summing) are compared to those obtained using the procedure described in Imbriani *et al.* [25] and are shown in Fig. 2. The full-energy peak (without summing) and total efficiencies from the analysis are also shown.

The yields of the $\gamma$ rays corresponding to primary transitions to the ground state GS ($\gamma_0$), 1.37 ($\gamma_1$), 4.12 ($\gamma_2$), 4.24 ($\gamma_3$), 5.23 ($\gamma_4$), 6.01 ($\gamma_5$), 8.44, and 10.73 MeV excited states were determined from the spectra. An example off-resonance spectrum at $E_p = 879$ keV, where the strongest transitions are indicated, is given in Fig. 3. The thicknesses of the evaporated targets were determined through (a) scans of the narrow resonances at 309 and 510 keV and (b) from the width of the observed primary $\gamma$ peaks at beam energies for which the cross section only varies slowly over the beam energy range in the target (i.e., off resonance). Secondary peaks were found to be heavily affected by diffusion of sodium into deeper layers of the targets. Although this effect was found to be smaller in targets with less time between evaporation and measurement, due to the difficulties in correcting for this effect, secondary peaks were not evaluated. The differential cross sections for the primary capture transitions were determined by fitting the primary $\gamma$-ray peaks, considering the variation of the yield
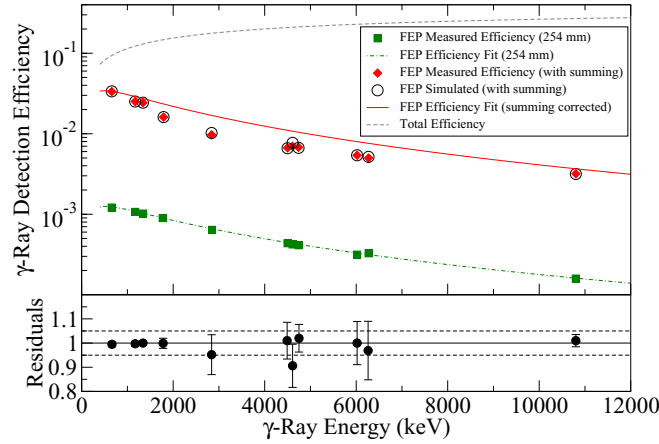
FIG. 2. The top panel shows a comparison between close geometry (red) and far geometry (254 mm, green) measurements of the $\gamma$-ray full-energy peak detection efficiency. Both data sets include the effects of summing, but in the far geometry they are negligible. The solid lines indicate empirical fits to the data where the summing is either negligible (far geometry) or has been corrected as described in Imbriani *et al.* [25]. The total efficiency is indicated by the dashed grey line. The bottom panel gives the residuals between the measured and simulated full-energy peak efficiencies (with summing) in close geometry.

due to the thickness of the target using the methods described in Di Leva *et al.* [26], and are shown in Figs. 4 and 5. The data are given in the Supplemental Material [27].
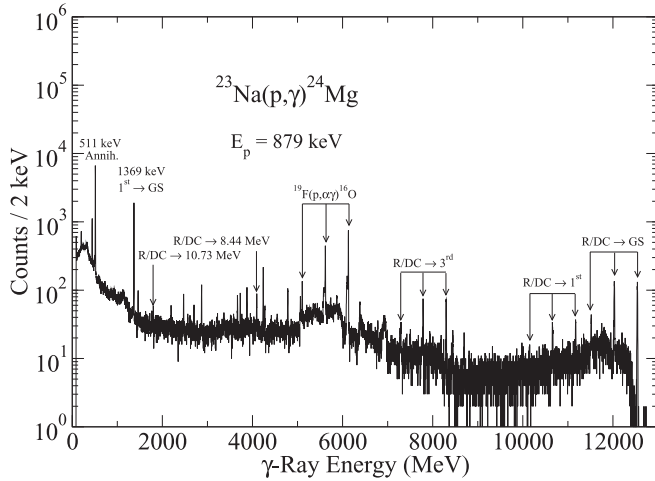


FIG. 3. An off-resonance $\gamma$-ray spectrum at $E_p = 879$ keV. The strongest transitions (the full-energy peak and two escape peaks where they are visible) of the $^{23}$Na$(p, \gamma)$$^{24}$Mg reaction are indicated. A strong background peak is observed from the $^{19}$F$(p, \alpha\gamma)$$^{16}$O reaction, owing to fluorine contamination in the Ta backing. Transitions are indicated for both primary resonance (R) or direct capture (DC) to different final states (indicated by the number of the excited state for low lying states) as well as the strong secondary transition from the first excited state to the ground state (GS). The line at 511 keV due to electron-positron annihilation is also indicated.

## IV. *R*-MATRIX ANALYSIS

An *R*-matrix analysis was performed for the experimental data over the energy regions exhibiting broad resonances or direct capture contributions using the code AZURE2 [29,30]. The alternative *R*-matrix parametrization of Brune [31] was utilized in order to work directly with observable energies and partial widths and to remove the need for boundary conditions. For bound states, the strength of the external capture is parametrized in terms of ANCs. Channel radii of $a_p = 6.0$ fm and $a_\alpha = 6.5$ fm were adopted for the proton and $\alpha$-particle channels, respectively. Masses and separation energies were taken from the mass evaluation [32,33]. For all of the transitions observed, $E1$ multipolarity dominates for the direct contribution to the cross section.

Over the energy range of interest, levels populated by proton capture in the $^{24}$Mg compound nucleus can particle decay to the ground state and first excited state of $^{23}$Na and $^{20}$Ne through proton and $\alpha$ emission, respectively. However, the total widths of the levels populated in the present $^{23}$Na$(p, \gamma)$$^{24}$Mg data are dominated by deexcitation through their ground state proton widths. An additional resonance, excited in the $^{23}$Na$(p, p_0)$$^{23}$Na data, also has a substantial ground state $\alpha$-particle width. Therefore, only the ground state proton and $\alpha$-particle partitions are included in the *R*-matrix analysis. For the $\gamma$-ray partitions, only the observed transitions to the ground state ($J^\pi = 0^+$), first ($E_x = 1.369$ MeV, $2^+$), second (4.123 MeV, $4^+$), third (4.238 MeV, $2^+$), fourth (5.235 MeV, $3^+$), fifth (6.011 MeV, $4^+$), and two high-lying (8.437 MeV, $1^-$ and 10.731 MeV, $2^+$) excited states are included.

Previous data from the literature over the energy range under investigation are quite limited. There are many measurements of the $^{23}$Na$+p$ reactions at lower energies, characterizing narrow resonance strengths, but most cross section measurements begin at energies above the current data. The broad resonances observed here correspond to those seen in the $^{23}$Na$(p, p_0)$$^{23}$Na elastic scattering data of Baumann *et al.* [28]. These are the only proton scattering data reported over this energy range. In $\alpha$ scattering, the data of Goldberg *et al.* [34] cover the corresponding excitation energy range, but since the resonances observed in the $^{23}$Na$+p$ data correspond to levels with total widths dominated by their ground state proton widths, they do not appear as resonances in the $\alpha$-scattering data. An *R*-matrix fit to the $^{23}$Na$(p, p_0)$$^{23}$Na data of Baumann *et al.* [28] and to the $^{23}$Na$(p, \gamma)$$^{24}$Mg primary capture data of the present work is shown in Figs. 4 and 5.

The parameters varied in the *R*-matrix fit are summarized in Table I. The experimental data for GS, 1.37 ($\gamma_1$), 4.24 ($\gamma_3$), and 8.44 MeV transitions could be reproduced by just resonances arising from the two broad unnatural parity resonances at $E_x = 12.53$ ($1^+$) and 12.67 ($2^-$) MeV as well as interference from background contributions in some cases. On the other hand, the data for the transitions to the excited states at 4.12 ($\gamma_2$), 5.23 ($\gamma_4$), and 6.01 MeV could be described using only hard-sphere external capture (EC) to model the DC. Only the transition at 10.731 MeV shows a measurable mixture of resonance and direct contributions, having a resonance that corresponds to the $E_x = 12.53$ ($1^+$) state and flat
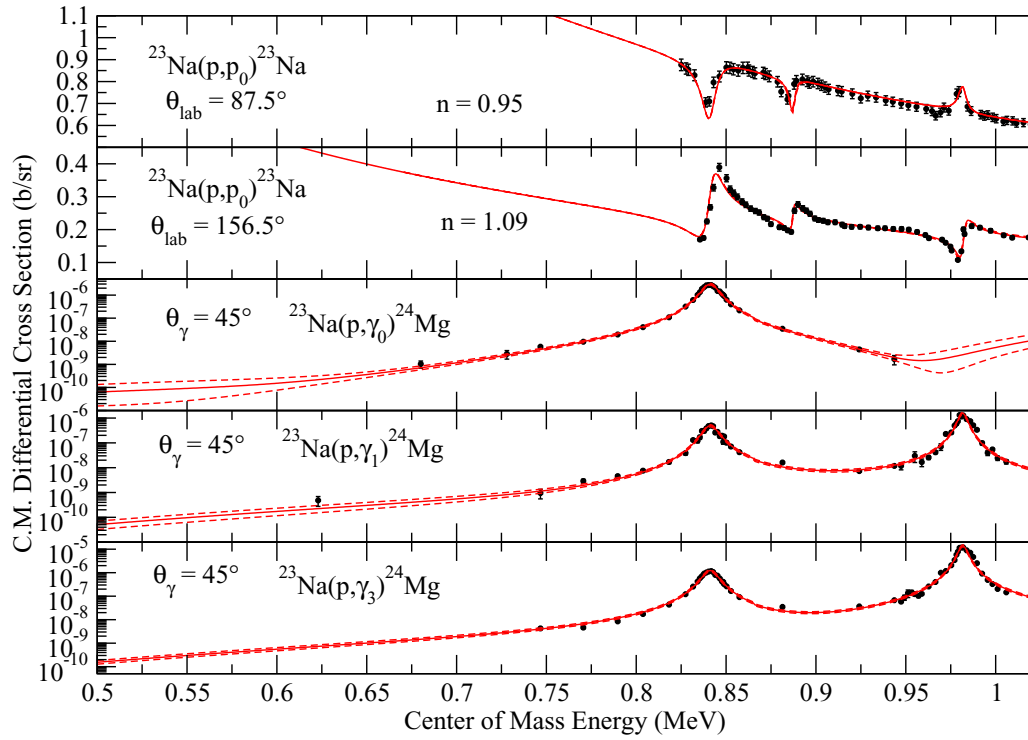
FIG. 4. *R*-matrix fit to the $^{23}$Na$(p, p_0)^{23}$Na data of Baumann *et al.* [28] and the $^{23}$Na$(p, \gamma_{0,1,3})^{24}$Mg data of the present work. The solid red lines indicate the best fit (50% quantile) while the dashed red lines indicate the 16% and 84% quantiles found from the MCMC analysis. The "n" in the two upmost plots are normalization factors; see Table I.
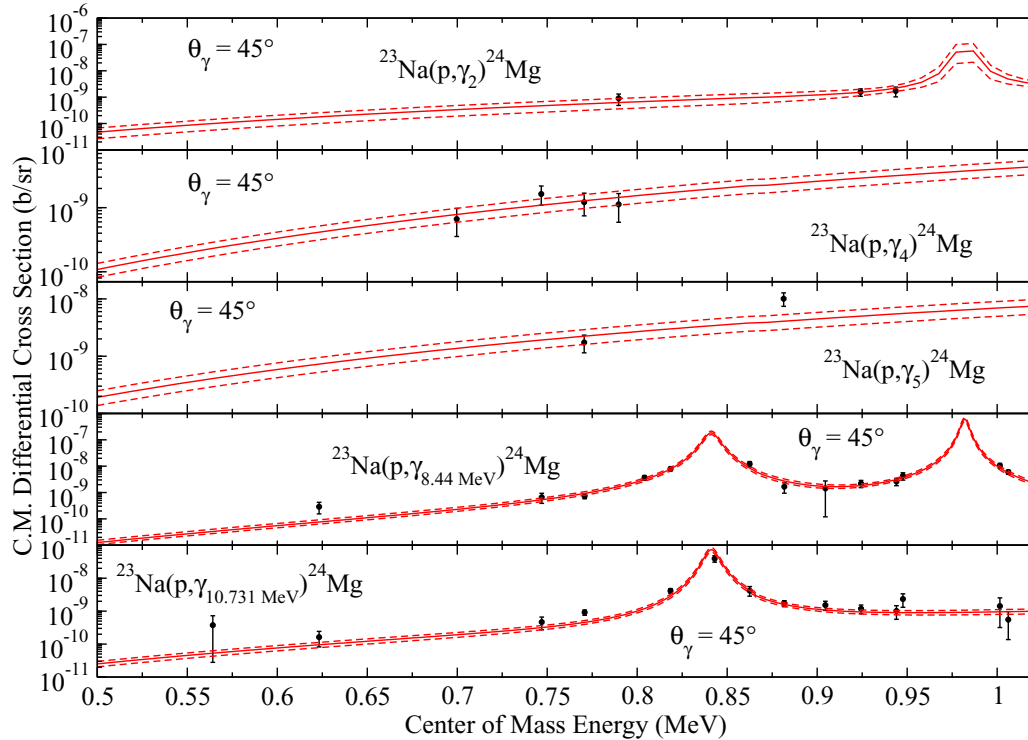


FIG. 5. As in Fig. 4, except for the $^{23}$Na$(p, \gamma_{2,4,5,8.44 \text{ MeV},10.37 \text{ MeV}})^{24}$Mg cross sections.

TABLE I. Best fit parameters for the MCMC analysis using the Python package EMCEE implemented in the $R$-matrix code AZURE2 with the Python package BRICK. The signs on the partial widths indicate the sign of the corresponding reduced width amplitude. Upper limits correspond to a 68% confidence limit.

| $E_{c.m.}$ (keV) | $E_x$ (keV) | $J^\pi$ | $\Gamma_p$ or ANC | $\Gamma_{\gamma_0}$ | $\Gamma_{\gamma_1}$ | $\Gamma_{\gamma_3}$ (eV) or (fm$^{-1/2}$) | $\Gamma_{8.44\ \mathrm{MeV}}$ | $\Gamma_{10.73\ \mathrm{MeV}}$ | $\Gamma_\alpha$ |
|---|---|---|---|---|---|---|---|---|---|
| **Bound states** | | | | | | | | | |
| | 0[a] | $0^+$ | $<52$ | | | | | | |
| | 1.3687[a] | $2^+$ | $<-25$ | | | | | | |
| | 4.1229[a] | $4^+$ | $<8$ | | | | | | |
| | 4.2382[a] | $2^+$ | $<22$ | | | | | | |
| | 5.2351[a] | $3^+$ | $<11$ | | | | | | |
| | 6.0108[a] | $4^+$ | $<11$ | | | | | | |
| | 8.4373[a] | $1^-$ | $<7$ | | | | | | |
| | 10.7308[a] | $2^+$ | $3.81(37)$ | | | | | | |
| **Unbound states** | | | | | | | | | |
| 841.2 | 12.5339(1) | $1^+$ | $9270(110)$ | $0.292(28)$ | $0.0491(48)$ | $0.113(12)$ | $0.018(3)$ | $7(1)\times10^{-3}$ | |
| 887.1 | 12.5798(2) | $2^+$ | $1150(120)$ | | | | | | $-2900(500)$ |
| 981.5 | 12.6745(1) | $2^-$ | $4000(100)/660(70)$ | | $-0.062(6)$ | $0.54(6)$ | $-0.015(6)/0.095(5)$ | | |
| **Background states** | | | | | | | | | |
| | 13[a] | $1^+$ | $6.7(2)\times10^4$ | $20(10)$ | | | | | |
| | 13.1[a] | $2^-$ | $[-3.0(2)/-3.7(2)]\times10^4$ | | | | | | |
| | 30[a] | $1^+$ | $5\times10^{7}$[a] | $-2(1)\times10^4$ | | | | $-3.6(5)\times10^4$ | |

Normalization factors

$n_{\mathrm{Baumann},\theta_{lab}=87.5°} = 0.95^{+0.03}_{-0.03}$

$n_{\mathrm{Baumann},\theta_{lab}=156.5°} = 1.09^{+0.06}_{-0.06}$

[a]Fixed parameter.

off-resonance $S$ factor indicative of direct capture. A break down of the $R$-matrix reaction components for the fit to the $E_x = 10.731$ MeV final state transition is shown in Fig. 6. The $R$-matrix parameters for the best fit are given in Table I.

Note that there are two closely spaced bound states in $^{24}$Mg at $E_x = 8.357\,98(13)$ and $8.437\,31(15)$ with $J^\pi = 1^-$ and $4^+$, respectively. It has been assumed that the observed transition yield reported here for the $E_x = 8.44$ MeV transition is dominated by the $1^-$ transition. This is suggested by the calculation of the DC cross sections for the two transitions from the $C^2S$ values of Garrett *et al.* [16]. It is possible that the yield over the resonance could have significant contributions for the $4^+$ transition, as that can be populated through an $E2$ transition.

### A. MCMC uncertainty analysis

In the $R$-matrix fit described in Sec. IV, the present data could be described as a mixture of resonance and EC contributions. For some transitions, resonance contributions alone were sufficient to describe the experimental data. However, to obtain upper limits for the DC of these transitions, an EC contribution was included in every transition.

An MCMC uncertainty analysis was performed on the $R$-matrix fit using the Bayesian $R$-matrix Inference Code Kit (BRICK) [35]. BRICK provides communication between the MCMC Python routine EMCEE [36] and the C + + $R$-matrix code AZURE2 [29,30]. The MCMC routine requires priors for the $R$-matrix fit and normalization parameters. For the $R$-matrix fit parameters, uniform priors were taken, while for the normalization factors a Gaussian prior with a $\sigma = 10\%$ was used for both the scattering and capture data based on the systematic uncertainty information found in the present work and in Baumann *et al.* [28]. The parameter posteriors and correlations calculated by EMCEE are provided as a corner plot [37] in the Supplemental Material [27] and the 68% confidence level uncertainties are given in Table I.

As described in Sec. IV, the cross section measurements for many of the observed transitions provided only upper limits for the external capture contribution. The upper limits (68%
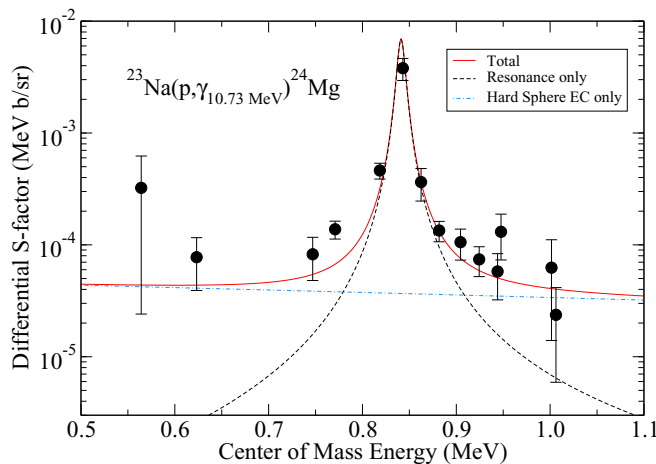


FIG. 6. $R$-matrix components used to fit the primary transition to the $E_x = 10.73$ MeV final state in the $^{23}$Na$(p, \gamma)^{24}$Mg reaction. The experimental data indicate the presence of both a single resonance, corresponding to the unbound state at $E_x = 12.53$ MeV, and external capture, modeled using $E1$ multipolarity only.

TABLE II. Summary of the upper limits (68% confidence) for the ANCs, reduced width amplitudes, and dimensionless reduced proton widths for the final states in $^{24}$Mg of the transitions observed in the present study. A Wigner limit of $\gamma_{(\text{Wigner})} = 1.34$ MeV$^{1/2}$ was used.

| $E_x$ (MeV) | $J^\pi$ | ANC (fm$^{-1/2}$) | $\gamma$ (MeV$^{1/2}$) | $\theta^2$ |
|---|---|---|---|---|
| 0 | $0^+$ | < 52 | <0.70 | <0.27 |
| 1.369 | $2^+$ | <25 | <0.23 | <0.029 |
| 4.123 | $4^+$ | <8 | <0.23 | <0.029 |
| 4.238 | $2^+$ | <22 | <0.33 | <0.060 |
| 5.235 | $3^+$ | <11 | <0.41 | <0.093 |
| 6.011 | $4^+$ | <11 | <0.50 | <0.14 |
| 8.437 | $1^-$ | <7 | <0.31 | <0.053 |
| 10.731 | $2^+$ | 3.81(37) | 0.14 | 0.011 |

confidence) for the ANCs, which were used to parametrize the strength of the external capture, for each of the observed $\gamma$-ray transitions are given in Table I. The dimensionless reduced width can be used to provide an approximate measure of the single particle or cluster nature of a state [38] and is given by

$$\theta^2 = \gamma^2/\gamma_W^2, \tag{1}$$

where $\gamma^2$ is the observable reduced width and $\gamma_W^2$ is the Wigner limit

$$\gamma_W^2 = 3\hbar^2/2\mu a^2. \tag{2}$$

Here $\mu$ is the reduced mass and $a$ is the channel radius. A pure single particle or cluster state corresponds to $\theta_\alpha^2 \approx 1$. The upper limits for the dimensionless reduced width amplitudes for the observed transitions of this work are given in Table II. The largest $\theta^2$ upper limits are found for the ground state and the fifth excited state, but even these upper limits are significantly smaller than 1.

The posteriors for the normalization factors of the capture data from the present work returned their priors, indicating, as expected, that there are no other constraints present in the model that determine the absolute scale of the capture cross section. On the other hand, the posteriors for the scattering data normalization factors are somewhat different from their priors, giving both a different central value and a much smaller uncertainty. This results from the $R$-matrix model calculation of the Coulomb scattering cross section and the presence of large amounts of data where this theoretically constrained portion of the cross section dominates in off-resonance regions (see Fig. 4). While the normalization factors produce somewhat different cross sections to those given by Baumann *et al.* [28], they are within the 10% systematic uncertainty estimated in that work (see Table I). It is always possible that there could be a significant modification to the low energy Coulomb scattering cross section from broad resonances or other background sources. Additional scattering data, with comprehensive angular coverage, are required in order to make more definitive conclusions.
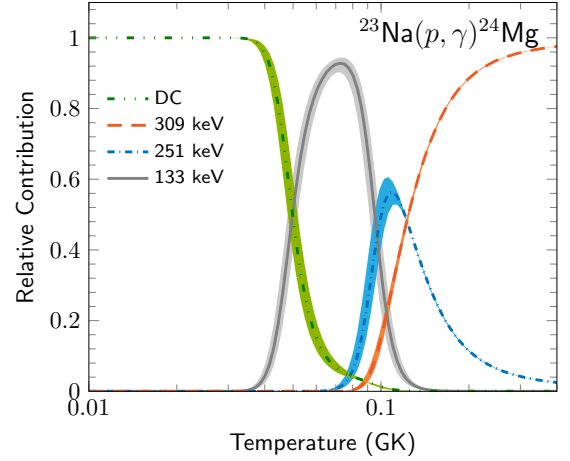


FIG. 7. Relative contributions to the total reaction rate over the low temperature region where the rate is dominated by the DC and resonances at $E_p = 133$, 251, and 309 keV.

## V. DC CALCULATIONS

The proton separation energy in $^{24}$Mg is $S_p = 11.69$ MeV, with more than 60 known proton bound states. Further, proton $C^2S$ values from transfer studies indicate that the DC deexcitation is rather evenly distributed [13,15,16] (see Sec. I), indicating a rather homogeneous distribution of the single-particle strength. This was reflected in the $\theta^2$ upper limits found from the $R$-matrix analysis in Sec. IV A, where all the $\theta^2 \ll 1$. Thus the $^{23}$Na$(p, \gamma)^{24}$Mg reaction requires the measurement of several individual transitions in order to characterize the total DC.

Figure 7 summarizes the fractional contributions from the different reaction components that make up the total $^{23}$Na$(p, \gamma)^{24}$Mg reaction rate at low temperatures. Below $\approx$0.04 GK, nonresonant capture dominates, as reported by several recent calculations that have used a similar nonresonant $S$factor [6,39,40]. A rate calculation was also reported in the NACRE compilation [41], but there the importance of the DC contribution was not realized, thus the nonresonant component was greatly underestimated. The transfer study of Hale *et al.* [42] was focused on levels near the proton separation energy, thus their calculations of the DC also continued to relied on previously measured proton $C^2S$ values compiled by Endt [43], coming from previous $(d, n)$ and $(^3\text{He}, d)$ transfer reactions [13–16]. The $C^2S$ values have uncertainties of $\approx$30–50% [16], which translate directly to the uncertainties in the DC $S$ factors and the DC contribution to the reaction rate below $\approx$0.04 GK.

Detailed comparisons of the individual transition $S$ factors of this work with past calculations cannot be made because previous works only reported the total $S$ factor (sum over all final states). However, these past works all calculated their DC contributions using a potential model to obtain a single-particle $S$ factor that was then weighted by the $C^2S$ values from the evaluation [43], which come mainly from Garrett *et al.* [16]. As the potential model parameters were all well documented, these calculations could be readily repeated for
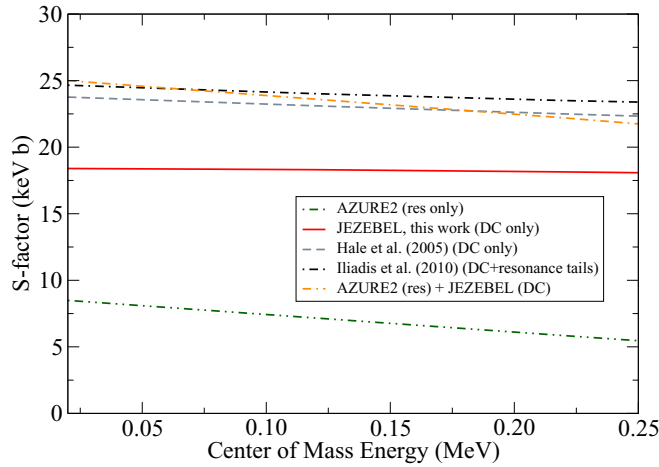
FIG. 8. Comparison of different total nonresonant $S$-factor calculations for the $^{23}$Na$(p, \gamma)^{24}$Mg reaction. The JEZEBEL calculations from this work (red solid line) and those of Hale *et al.* [42] (grey dashed line) represent potential model DC $S$ factors. That of Iliadis *et al.* [39] (black dashed-dotted line) is a "nonresonant" calculation including both DC and the tails of higher energy broad resonances. The resonant-only $S$ factor from the $R$-matrix calculation is also shown (green double-dotted-dashed line), as well as the sum of it and the JEZEBEL calculation (yellow dash-dash-dotted line).

the individual states with $C^2S$ values larger than 0.1 (see Fig. 1).

The single-particle DC $S$ factors ($S_{\rm sp}$) have been calculated using the potential model code JEZEBEL [44]. The DC $S$ factors

($S_{\rm DC}$) were then calculated as

$$(2J + 1)S_{\rm DC} = (2J + 1)C^2S \times S_{\rm sp}, \qquad (3)$$

using the $(2J + 1)C^2S$ values from Table VIII of Garrett *et al.* [16] and the level spins ($J$) from the compilation [45]. For comparison, the sum of these individual transitions is compared with the DC $S$ factor given by Hale *et al.* [42] and the nonresonant $S$ factor (which also contains high energy resonant tail contributions) from Iliadis *et al.* [39] in Fig. 8.

The nonresonant $S$-factors' upper limits determined from the $R$-matrix fit upper limits were found to be, for the most part, consistent with those calculated using the potential model and $C^2S$ values. In most transitions observed here, the constraints on the nonresonant $S$-factor from the transfer reaction $C^2S$ values were still more stringent, as illustrated in Figs. 9 and 10. Notably, for the $E_x = 10.73$ MeV transition, it has been found that an external capture component was statistically significant in order to achieve a good fit. The experimental data indicated a nonresonant $S$ factor smaller than that of the transfer reaction $C^2S$ by $\approx 50\%$. Therefore, the uncertainty for the overall nonresonant components of the $S$-factor have been increased from the 30–40% uncertainty estimated by Garrett *et al.* [16] to 50%.

## VI. REACTION RATE CALCULATIONS

For the narrow resonance contributions, strengths and energies have been taken from Boeltzig *et al.* [6], except for the energy of the lowest known resonance that was recently revised by Marshall *et al.* [46]. At temperatures below
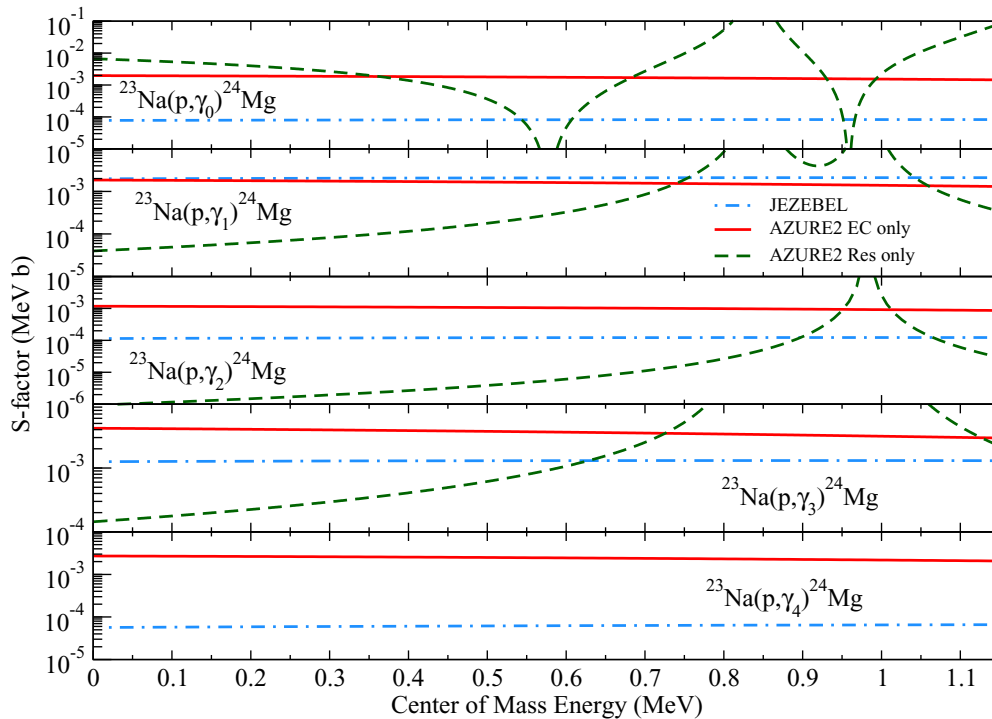


FIG. 9. Comparisons of the hard sphere external capture $S$ factors calculated from AZURE2 using the upper limit ANCs determined in this work, given in Table I (red line), to the direct capture $S$ factors calculated using $C^2S$ values from Garrett *et al.* [16] and the potential model code JEZEBEL (blue dashed-dotted line).
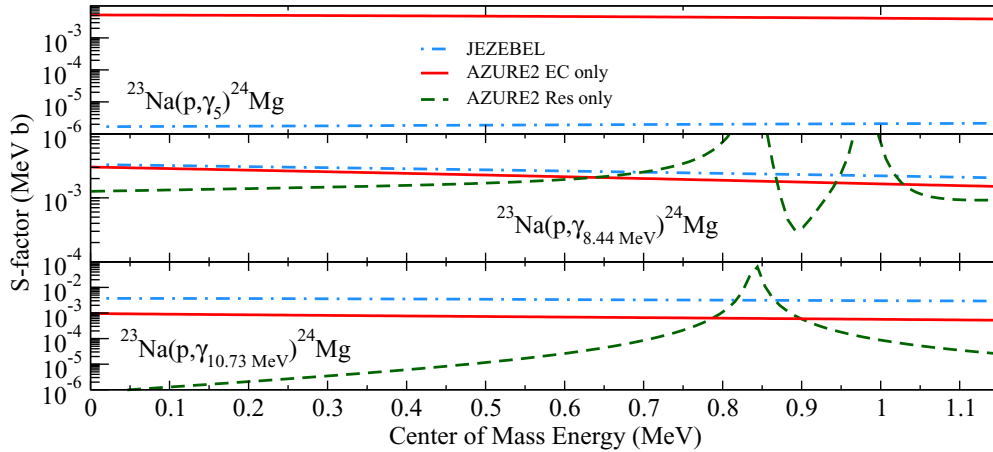
FIG. 10. As Fig. 9 but for the transition to the fifth excited state in $^{24}$Mg and the two high lying bound states at $E_x = 8.44$ and 10.73 MeV.

$\approx 0.04$ GK, the direct capture and broad resonance tail contributions studied in this work dominate the reaction rate, as shown in Fig. 7. The nonresonant portion of the reaction rate and its uncertainties were calculated as follows:

(i) The median rate weas determined using the $S$ factors calculated using JEZEBEL (see Sec. V). The present results are found to be about $\approx 20\%$ lower than previous calculations.

(ii) The lower limit was calculated using a 50% uncertainty for the $C^2S$ values and applying this to the JEZEBEL $S$ factors.

(iii) The upper limit was likewise calculated using a 50% uncertainty for the $C^2S$ values and applying this to the JEZEBEL $S$ factors. An additional contribution was also added for the ground state transition, where it was found in the $R$-matrix fit that the resonance tails of the ground state transition can make a significant contribution (see Sec. IV).

As shown in Fig. 11, the present reaction rate has a central value that is about 20% less than than that given recently by Marshall *et al.* [46], but remains within their uncertainty range. This lower value is likely the result of differences in the potential model codes used and adopted $C^2S$ values. The present study finds somewhat larger uncertainties, which can be attributed to the present study's inclusion of the interference uncertainty of the ground state transition and a larger uncertainty in the $C^2S$ values than that taken in previous calculations (50% instead of 30%).

## VII. SUMMARY

The present study reports cross section measurements for eight individual transitions of the $^{23}$Na$(p, \gamma)^{24}$Mg reaction over the laboratory energy range from $E_p = 0.5$ to 1.05 MeV for the first time. Two broad resonances were observed, whose low energy tails have substantial contributions to the nonresonant $S$ factor at low energy. Upper limits were also determined for the external capture contributions for each transition through an $R$-matrix analysis, which was then compared with DC $S$ factors calculated using a potential model and $C^2S$ values from a transfer measurement. The two methods were found to produce consistent nonresonant $S$ factors, and rather evenly distributed decay through several transitions was observed. Finally, direct capture in the $^{23}$Na$(p, \gamma)^{24}$Mg reaction was observed for the first time through the $E_x = 10.73$ MeV transition. Direct measurements with greater off-resonance sensitivity are needed in order to improve the constraint of the several other transitions that make significant contributions to the total off-resonance capture cross section. A transfer measurement to determine bound state ANCs is also highly recommended.
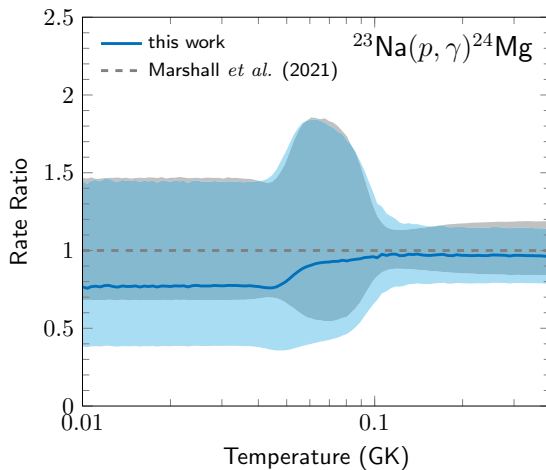


FIG. 11. Ratio of the present rate (blue solid line) and uncertainty (blue shaded region) to the median of Marshall *et al.* [46]. The relative uncertainties of Marshall *et al.* [46] (gray shaded region) are also shown for comparison.

[1] J. B. Marion and W. A. Fowler, Nuclear reactions with the neon isotopes in stars, Astrophys. J. **125**, 221 (1957).

[2] J. Goerres, M. Wiescher, and C. Rolfs, Hydrogen burning of $^{23}$Na in the NeNa cycle, Astrophys. J. **343**, 365 (1989).

[3] M. Arnould, S. Goriely, and A. Jorissen, Non-explosive hydrogen and helium burnings: abundance predictions from the NACRE reaction rate compilation, Astron. Astrophys. **347**, 572 (1999).

[4] R. G. Izzard, M. Lugaro, A. I. Karakas, C. Iliadis, and M. van Raai, Reaction rate uncertainties and the operation of the NeNa and MgAl chains during HBB in intermediate-mass AGB stars, Astron. Astrophys. **466**, 641 (2007).

[5] J. Jose, A. Coc, and M. Hernanz, Nuclear uncertainties in the NeNa-MgAl cycles and production of $^{26}$Al during nova outbursts, Astrophys. J. **520**, 347 (1999).

[6] A. Boeltzig, A. Best, F. Pantaleo, G. Imbriani, M. Junker, M. Aliotta, J. Balibrea-Correa, D. Bemmerer, C. Broggini, C. Bruno, R. Buompane, A. Caciolli, F. Cavanna, T. Chillery, G. Ciani, P. Corvisiero, L. Csedreki, T. Davinson, R. deBoer, R. Depalo *et al.*, Direct measurements of low-energy resonance strengths of the $^{23}$Na$(p, \gamma)^{24}$Mg reaction for astrophysics, Phys. Lett. B **795**, 122 (2019).

[7] Z. Switkowski, R. O'Brien, A. Smith, and D. Sargood, Total yield measurements in $^{23}$Na$(p, \gamma)^{24}$Mg, Aust. J. Phys. **28**, 141 (1975).

[8] A. M. Baxter, K. J. Cassell, and J. A. Kuehner, Resonance strengths and decay schemes in $^{23}$Na$(p, \gamma)^{24}$Mg, Can. J. Phys. **47**, 2319 (1969).

[9] F. Leccia, M. Aléonard, D. Castéra, P. Hubert, and P. Mennrath, Rapports d'embranchement, vies moyennes et mélanges multipolaires dans le noyau $^{24}$Mg, J. Phys. France **34**, 147 (1973).

[10] W. G. Mourad, Jr., K. Nielsen, and M. Petrilak, Precise measurement of relative energy positions and widths of some $(p, \gamma)$ resonances in aluminium and sodium, Nucl. Phys. A **102**, 406 (1967).

[11] M. Meyer, J. Reinecke, and D. Reitmann, A study of the $^{23}$Na$(p, \gamma)^{24}$Mg reaction and the excited states of $^{24}$Mg, Nucl. Phys. A **185**, 625 (1972).

[12] P. Endt, C. Alderliesten, F. Zijderhand, A. Wolters, and A. Van Hees, Spectroscopic information on $^{24}$Mg and $^{28}$Si from proton capture, Nucl. Phys. A **510**, 209 (1990).

[13] H. Fuchs, K. Grabisch, P. Kraaz, and G. Räschert, Study of $^{24}$Mg by the $^{23}$Na$(d, n)$ reaction at $E_d = 6$ MeV, Nucl. Phys. A **122**, 59 (1968).

[14] S. Tang, B. Sowerby, and D. Sheppard, Study of levels in $^{24}$Mg by the $^{23}$Na$(d, n)^{24}$Mg reaction, Nucl. Phys. A **125**, 289 (1969).

[15] R. C. Bearse and J. L. Yntema, Study of the $^{23}$Na$(^3$He$, d)^{24}$Mg reaction, Phys. Rev. **175**, 1442 (1968).

[16] J. D. Garrett, H. T. Fortune, R. Middleton, and W. Scholz, Nuclear structure of $^{24}$Mg: $^{23}$Na$(^3$He$, d)$ reaction, Phys. Rev. C **18**, 2032 (1978).

[17] C. Rolfs, Spectroscopic factors from radiative capture reactions, Nucl. Phys. A **217**, 29 (1973).

[18] A. M. Lane and R. G. Thomas, R-matrix theory of nuclear reactions, Rev. Mod. Phys. **30**, 257 (1958).

[19] R. J. Holt, H. E. Jackson, R. M. Laszewski, J. E. Monahan, and J. R. Specht, Effects of channel and potential radiative transitions in the $^{17}$O$(\gamma, n_0)^{16}$O reaction, Phys. Rev. C **18**, 1962 (1978).

[20] F. C. Barker and T. Kajino, The $^{12}$C$(\alpha, \gamma)^{16}$O cross section at low energies, Aust. J. Phys. **44**, 369 (1991).

[21] C. Angulo and P. Descouvemont, The $^{14}$N$(p, \gamma)^{15}$O low-energy $S$-factor, Nucl. Phys. A **690**, 755 (2001).

[22] R. J. deBoer, J. Görres, M. Wiescher, R. E. Azuma, A. Best, C. R. Brune, C. E. Fields, S. Jones, M. Pignatari, D. Sayre, K. Smith, F. X. Timmes, and E. Uberseder, The $^{12}$C$(\alpha, \gamma)^{16}$O reaction and its implications for stellar helium burning, Rev. Mod. Phys. **89**, 035007 (2017).

[23] A. M. Mukhamedzhanov, C. A. Gagliardi, and R. E. Tribble, Asymptotic normalization coefficients, spectroscopic factors, and direct radiative capture rates, Phys. Rev. C **63**, 024612 (2001).

[24] A. Antilla, J. Keinonen, M. Hautala, and I. Forsblom, Use of the $^{27}$Al$(p, \gamma)^{28}$Si, $E_p = 992$ keV resonance as a gamma-ray intensity standard, Nucl. Instrum. Methods **147**, 501 (1977).

[25] G. Imbriani, H. Costantini, A. Formicola, A. Vomiero, C. Angulo, D. Bemmerer, R. Bonetti, C. Broggini, F. Confortola, P. Corvisiero, J. Cruz, P. Descouvemont, Z. Füläp, G. Gervino, A. Guglielmetti, C. Gustavino, G. Gyürky, A. P. Jesus, M. Junker, J. N. Klug *et al.*, $S$ factor of $^{14}$N$(p, \gamma)^{15}$O at astrophysical energies, Eur. Phys. J. A **25**, 455 (2005).

[26] A. Di Leva, D. A. Scott, A. Caciolli, A. Formicola, F. Strieder, M. Aliotta, M. Anders, D. Bemmerer, C. Broggini, P. Corvisiero, Z. Elekes, Z. Fülöp, G. Gervino, A. Guglielmetti, C. Gustavino, G. Gyürky, G. Imbriani, J. José, M. Junker, M. Laubenstein *et al.* (LUNA Collaboration), Underground study of the $^{17}$O$(p, \gamma)^{18}$F reaction relevant for explosive hydrogen burning, Phys. Rev. C **89**, 015803 (2014).

[27] See Supplemental Material at http://link.aps.org/supplemental/10.1103/PhysRevC.106.045801 for tabulated experimental data and a corner plot of the covariance matrix for the $R$-matrix parameters.

[28] N. P. Baumann, F. W. Prosser, W. G. Read, and R. W. Krone, Elastic scattering of protons from $^{23}$Na, Phys. Rev. **104**, 376 (1956).

[29] R. E. Azuma, E. Uberseder, E. C. Simpson, C. R. Brune, H. Costantini, R. J. de Boer, J. Görres, M. Heil, P. J. LeBlanc, C. Ugalde, and M. Wiescher, AZURE: An $R$-matrix code for nuclear astrophysics, Phys. Rev. C **81**, 045805 (2010).

[30] E. Uberseder and R. J. deBoer, *AZURE2 User Manual* (2015), http://azure.nd.edu.

[31] C. R. Brune, Alternative parametrization of $R$-matrix theory, Phys. Rev. C **66**, 044611 (2002).

[32] W. Huang, G. Audi, M. Wang, F. G. Kondev, S. Naimi, and X. Xu, The AME2016 atomic mass evaluation (I). Evaluation of input data and adjustment procedures, Chin. Phys. C **41**, 030002 (2017).

[33] M. Wang, G. Audi, F. G. Kondev, W. Huang, S. Naimi, and X. Xu, The AME2016 atomic mass evaluation (II). Tables, graphs and references, Chin. Phys. C **41**, 030003 (2017).

[34] E. Goldberg, W. Haeberli, A. I. Galonsky, and R. A. Douglas, Elastic scattering of alpha particles by neon, Phys. Rev. **93**, 799 (1954).

[35] D. Odell, C. Brune, D. Phillips, R. deBoer, and S. Paneru, Performing Bayesian analyses with AZURE2 using BRICK: an application to the $^7$Be system, Front. Phys. **10**, 888476 (2022).

[36] D. Foreman-Mackey, D. W. Hogg, D. Lang, and J. Goodman, emcee: The MCMC hammer, Publ. Astron. Soc. Pac. **125**, 306 (2013).

[37] D. Foreman-Mackey, corner.py: Scatterplot matrices in Python, J. Open Source Softw. **1**, 24 (2016).

[38] Y. Kanada-En'yo, T. Suhara, and Y. Taniguchi, Approximation of reduced width amplitude and application to cluster decay width, Prog. Theor. Exp. Phys. **2014**, 073D02 (2014).

[39] C. Iliadis, R. Longland, A. Champagne, and A. Coc, Charged-particle thermonuclear reaction rates: III. Nuclear physics input, Nucl. Phys. A **841**, 251 (2010), special issue, The 2010 Evaluation of Monte Carlo based Thermonuclear Reaction Rates.

[40] J. M. Cesaratto, A. E. Champagne, M. Q. Buckner, T. B. Clegg, S. Daigle, C. Howard, C. Iliadis, R. Longland, J. R. Newton, and B. M. Oginni, Measurement of the $E_r^{\text{c.m.}} = 138$ keV resonance in the $^{23}$Na$(p, \gamma)^{24}$Mg reaction and the abundance of sodium in AGB stars, Phys. Rev. C **88**, 065806 (2013).

[41] C. Angulo, M. Arnould, M. Rayet, P. Descouvemont, D. Baye, C. Leclercq-Willain, A. Coc, S. Barhoumi, P. Aguer, C. Rolfs, R. Kunz, J. Hammer, A. Mayer, T. Paradellis, S. Kossionides, C. Chronidou, K. Spyrou, S. Degl'Innocenti, G. Fiorentini, B. Ricci *et al.*, A compilation of charged-particle induced thermonuclear reaction rates, Nucl. Phys. A **656**, 3 (1999).

[42] S. E. Hale, A. E. Champagne, C. Iliadis, V. Y. Hansper, D. C. Powell, and J. C. Blackmon, Investigation of the $^{23}$Na$(p, \gamma)^{24}$Mg and $^{23}$Na$(p, \alpha)^{20}$Ne reactions via $(^3$He, $d)$ spectroscopy, Phys. Rev. C **70**, 045802 (2004).

[43] P. Endt, Energy levels of $A = 21$–44 nuclei (VII), Nucl. Phys. A **521**, 1 (1990).

[44] M. Wiescher, H. Becker, J. Gärres, K.-U. Kettner, H. Trautvetter, W. Kieser, C. Rolfs, R. Azuma, K. Jackson, and J. Hammer, Nuclear and astrophysical aspects of $^{18}$O$(p, \gamma)^{19}$F, Nucl. Phys. A **349**, 165 (1980).

[45] R. Firestone, Nuclear data sheets for $A = 24$, Nucl. Data Sheets **108**, 2319 (2007).

[46] C. Marshall, K. Setoodehnia, F. Portillo, J. H. Kelley, and R. Longland, New energy for the 133-keV resonance in the $^{23}$Na$(p, \gamma)^{24}$Mg reaction and its impact on nucleosynthesis in globular clusters, Phys. Rev. C **104**, L032801 (2021).